

# Tampering Detection and Localization through Clustering of Camera-Based CNN Features

Luca Bondi<sup>1</sup>, Silvia Lameri<sup>1</sup>, David Güera<sup>2</sup>, Paolo Bestagini<sup>1</sup>, Edward J. Delp<sup>2</sup>, Stefano Tubaro<sup>1</sup>

<sup>1</sup> Dipartimento di Elettronica, Informazione e Bioingegneria, Politecnico di Milano - Milano, Italy

<sup>2</sup> School of Electrical and Computer Engineering, Purdue University - West Lafayette, IN, USA

## Abstract

*Due to the rapid proliferation of image capturing devices and user-friendly editing software suites, image manipulation is at everyone's hand. For this reason, the forensic community has developed a series of techniques to determine image authenticity. In this paper, we propose an algorithm for image tampering detection and localization, leveraging characteristic footprints left on images by different camera models. The rationale behind our algorithm is that all pixels of pristine images should be detected as being shot with a single device. Conversely, if a picture is obtained through image composition, traces of multiple devices can be detected. The proposed algorithm exploits a convolutional neural network (CNN) to extract characteristic camera model features from image patches. These features are then analyzed by means of iterative clustering techniques in order to detect whether an image has been forged, and localize the alien region.*

## 1. Introduction

The widespread availability of image processing software, both for personal computers and smartphones, allows almost every user to modify and publish digital images. The kind of processing varies from visual enhancement tailored to improve viewing experience, to image combination and manipulation, with the goal of modifying image content's semantic. In order to restore faith in digital photography, in the last decade, a considerable number of works have addressed the problem of determining origin and authenticity of digital images [34, 35].

Detecting whether an image has been edited is possible as all non-invertible operations applied to a picture leave peculiar footprints, which can be detected to expose forgeries [31]. Among the many techniques developed in the image forensic literature, some are tailored to the detection of a single trace left by a specific operation on the whole pic-

ture (*i.e.* tampering detection). Other techniques focus on localizing regions that present traces of editing (*i.e.* tampering localization). As an example of algorithms belonging to the former category, [32, 19] present some techniques to expose traces of resampling. In [6, 20], the authors focused on detecting the use of median filter. In [28, 29], the authors presented the possibility of attributing a digital image to the camera used to shot it exploiting photo-response non uniformity (PRNU), even after different kinds of transformations [17]. Moreover, many works have been presented to study traces left by JPEG compression [3, 8, 38]. Considering tampering localization problem, copy-move forgeries detectors via keypoints matching [1], gaussian models and auto-encoders on co-occurrences of high-pass image components [41, 10], fusion of phylogeny, PRNU and patch matching techniques [15] are just a few examples of methods devoted to determine where manipulation occurred based on different footprints.

In this paper we address tampering detection and localization problem for images obtained through splicing of content originally shot from different camera models. Specifically, we analyze images in a patch-wise fashion, and aim to detect whether different patches belong to different camera models (*i.e.* the image has been forged) exploiting descriptors learned by a convolutional neural network (CNN) [4].

As a matter of fact, back in 1998, LeCun *et al.* [24] showed how CNNs applied to handwritten digits recognition could open a new era to computer vision. However, only starting from 2012 [23] the availability of fast and parallel computing devices (*e.g.* GPUs) really made CNNs at researchers' hands. AlexNet [23], Network in Network [26] and GoogLeNet [36] are just three examples of data-driven Deep Learning models that showed impressive accuracy improvements in image classification and localization tasks over the previously widespread handcrafted features [37, 18, 39]. In the last few years, image forensics and Deep Learning started to talk. Chen *et al.* [7] and Qian *et al.* [33] worked respectively on CNN tailored to me-

dian filtering detection and steganalysis, showing that also in forensic scenarios CNNs could improve state-of-the-art results. Generic image manipulation detection through high-pass enforced convolutional layers [2] has shown that forensic tasks might require some prior to be accounted for in a purely Deep Learning data-driven approach. More recently, video forgery detection [9] and camera model identification with CNNs [40, 4] showed that learning traces hidden behind image content is possible even when small image patches are considered.

Based on this idea, our image tampering detection and localization approach leverages descriptors learned for camera model identification using the convolutional neural network (CNN) proposed in [4]. These descriptors extracted from small image patches are analyzed by means of an iterative clustering technique to expose regions of an image that appear to be obtained from different camera models. Results obtained on 2 000 images in different conditions show that the proposed solution outperforms several state-of-the-art detectors [43].

The rest of the paper is structured as follows. Section 2 reports some background on image tampering localization and CNNs necessary to understand the rest of the work. Section 3 presents all details of the proposed algorithm. Section 4 reports all the performed experiments and the achieved results. Finally, Section 5 concludes the paper.

## 2. Background

Before addressing the problem of image tampering detection and localization exploiting recent results in camera model identification, in this section we provide the reader with some background on image tampering detection and localization, and on Convolutional Neural Networks for camera model identification.

### 2.1. Image Tampering Detection and Localization

Image tampering detection and localization techniques have been developed over time by a number of researchers focusing on copy-move forgeries, splice forgeries, inpainting, image-wise adjustments (resizing, histogram equalization, cropping, etc.) and many more. Following the survey presented by Zampoglou *et al.* [43], we provide an overview of the literature methods against which our algorithm will be compared. Specifically, we focus on algorithms that do not need any prior information (*e.g.* JPEG header, additional inputs such as reference PRNUs, etc.), and follow the naming convention used in [43] and the derived toolbox.

**ADQ1** Aligned Double Quantization detection, developed by Lin *et al.* in [27] aims at discovering the absence of double JPEG compression traces in tampered  $8 \times 8$  image blocks. Posterior probabilities for each block being possibly

tampered are generated through voting among discrete cosine transform (DCT) coefficients histograms collected for all blocks in the image.

**BLK** Due to its nature, JPEG compression introduces  $8 \times 8$  periodic artifacts on images that can be highlighted thanks to Block Artifact Grids (BAG) technique from Li *et al.* [25]. Detecting disturbances in the BAG allows to find traces of image cropping (grid misalignment), painted regions, copy-move portions.

**CFA1** At acquisition time, color images undergo Color Filter Array (CFA) interpolation due to the nature of acquisition process. Detecting anomalies in the statistics of CFA interpolation patterns allows Ferrara *et al.* [13] to build a tampering localization system. A mixture of Gaussian distributions is estimated from all the  $2 \times 2$  blocks of the image, resulting in a fine-grained tamper probability map.

**CFA2** By estimating CFA patterns within four common Bayer patterns, Dirik and Memon [11] show that if none of the candidate patterns fits sufficiently better than the other in a neighborhood, it is likely that tampering occurred. In fact, weak traces of interpolation left by the de-mosaicking algorithm are hidden by typical splicing operations like resizing and rotations.

**DCT** Inconsistencies in JPEG DCT coefficients histograms are detected in [42] by first estimating the quantization matrix from trusted image blocks, then evaluating suspicious areas with a blocking artifact measure (BAM).

**ELA** Error Level Analysis [22] aims to detect parts of the image that have undergone fewer JPEG compressions than the rest of the image. It works by intentionally re-saving the image at a known error rate and then computing the difference between the original and the re-compressed image. Local minima in image difference indicate original regions, whereas local maximums are symptoms of image tampering.

**GHO** JPEG Ghosts detection by Farid [12] is an effective technique to identify parts of the image that were previously compressed with smaller quality factors. The method is based on finding local minimum in the sum of squared differences between the image under analysis and its re-compressed version with varying quality factors.

**NOI1** Mahdian *et al.* [30] build their tampering detector upon the hypothesis that usually Gaussian noise is added to

tampered regions with the goal of deceiving classical image tampering detection algorithms. Modeling the local image noise variance through wavelet filtering, a segmentation method based on homogeneous noise levels is used to provide an estimate of the tampered regions within an image.

**NOI4** A statistical framework aimed at fusing several sources of information about image tampering is presented by Fontani *et al.* [14]. Information provided by different forensic tools yields to a global judgment about the authenticity of an image. Outcomes from several JPEG-based algorithms are modeled and fused using Dempster-Shafer Theory of Evidence, being capable of handling uncertain answers and lack of knowledge about prior probabilities.

## 2.2. CNN for Camera Model Identification

Convolutional Neural Networks are a complex non-linear interconnection of neurons inspired by biology of human vision system. Successfully used in object recognition, face identification, image segmentation, etc., the use of CNNs in forensics is relatively recent. Inspired by results obtained by Bondi *et al.* [4], we take the proposed CNN as a feature extractor for each patch of the input image. The structure of a CNN is divided into several blocks, called layers. Each layer  $\mathcal{L}_i$  takes as input either an  $H_i \times W_i \times P_i$  feature map or a feature vector of size  $P_i$  and produces as output either an  $H_{i+1} \times W_{i+1} \times P_{i+1}$  feature map or a feature vector of size  $P_{i+1}$ . Layer types used in this work are

- **Convolutional layer** Performs convolution, with stride  $S_h$  and  $S_w$  along first two axes, between input feature maps and a set of  $P_{i+1}$  filters with size  $K_h \times K_w \times P_i$ . Output feature maps have size  $H_{i+1} = \lfloor \frac{H_i - K_h + 1}{S_h} \rfloor$ ,  $W_{i+1} = \lfloor \frac{W_i - K_w + 1}{S_w} \rfloor$  and  $P_{i+1}$ .
- **Max-pooling layer** Performs maximum element extraction, with stride  $S_h$  and  $S_w$  along first two axes, from a neighborhood of size  $K_h \times K_w$  over each 2D slice of input feature map. Output feature maps have size  $H_{i+1} = \lceil \frac{H_i - K_h + 1}{S_h} \rceil$ ,  $W_{i+1} = \lceil \frac{W_i - K_w + 1}{S_w} \rceil$  and  $P_{i+1} = P_i$ .
- **Fully-connected layer** Performs dot multiplication between input feature vector (or flattened feature maps) and a weights matrix with  $P_{i+1}$  rows and  $P_i$  (or  $H_i \cdot W_i \cdot P_i$ ) columns. Output feature vector has  $P_{i+1}$  elements.
- **ReLU layer** Performs element-wise non linear activation. Given a single neuron  $x$ , it is transformed in a single neuron  $y$  with  $y = \max(0, x)$ .
- **Softmax layer** Turns an input feature vector to a vector with the same number of elements summing to 1. Given an input vector  $x$  with  $P_i$  neurons  $x_j$   $i \in [1, P_i]$ ,

each input neuron produces a corresponding output neuron  $y_j = \frac{e^{x_j}}{\sum_{k=1}^{P_i} e^{x_k}}$ .

The network proposed in [4] is an 11 layer CNN structured as follows.

- An RGB color input patch of size  $64 \times 64$  is fed as input to the first Convolutional layer with kernel size  $4 \times 4 \times 3$  producing 32 feature maps as output. Filtering is applied with stride 1.
- The resulting  $63 \times 63 \times 32$  feature maps are aggregated with a Max-Pooling layer with kernel size  $2 \times 2$  applied with stride 2, producing  $32 \times 32 \times 32$  feature maps.
- A second Convolutional layer with 48 filters of size  $5 \times 5 \times 32$  applied with stride 1 generates  $28 \times 28 \times 48$  feature maps.
- A Max-Pooling layer with kernel size  $2 \times 2$  applied with stride 2 produces a  $14 \times 14 \times 48$  feature maps.
- A third Convolutional layer with 64 filters of size  $5 \times 5 \times 48$  applied with stride 1 generates  $10 \times 10 \times 64$  feature maps.
- A Max-Pooling layer with kernel size  $2 \times 2$  applied with stride 2 produces a  $5 \times 5 \times 64$  feature map.
- A fourth Convolutional layer with 128 filters of size  $5 \times 5 \times 64$  applied with stride 1 generates a vector of 128 elements.
- A fully connected layer with 128 output neurons followed by a ReLU layer produces the 128 element feature vector.
- A last fully connected layer with  $N_{\text{cams}}$  output neurons followed by a Softmax layer acts as logistic regression classifier during CNN training phase.  $N_{\text{cams}}$  is the number of camera model used at CNN training stage.

As shown in [4], the trained CNN is able to extract meaningful information about camera models even from images belonging to cameras never used for training the network. This property is paramount for our proposed tampering detection and localization solution, as it enables exposing forgeries operated also with unknown camera models.

## 3. Proposed Method

In this section we present the proposed method for image forgery detection and localization in case of images generated through composition of pictures shot with different camera models. In this scenario, we consider that pristine images are pictures directly obtained from a camera. Conversely, forged images are those created taking a pristine

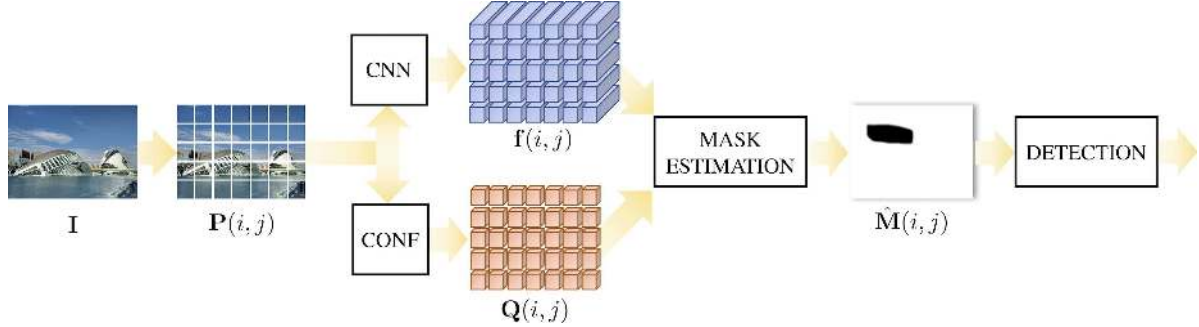


Figure 1. Pipeline of the proposed method. An image  $I$  is split into patches  $P(i, j)$ . Each patch is described by a feature vector  $f(i, j)$  extracted through a CNN, and a confidence score  $Q(i, j)$ . A custom clustering algorithm produces a tampering mask prediction  $\hat{M}$ , which is also used for detection.

image, and pasting onto it one or more small regions taken from pictures shot with different camera models with respect to the one used for the pristine shot. Under these assumptions, the proposed method is devised to estimate whether the totality of image patches come from a single camera (*i.e.* the image is pristine), or some portions of the image are not coherent with the rest of the picture in terms of camera attribution (*i.e.* the image is forged). If this is the case, we also localize the forged region.

Figure 1 outlines the proposed pipeline used to detect and localize tampered regions within images. An image  $I$  is first divided into non-overlapping patches. Each patch  $P$  is fed as input to a pre-trained CNN to extract a feature vector  $f$  of  $N_{\text{cams}}$  elements. Information about patch position, feature vectors  $f$  and patch confidence are given as input to the clustering algorithm that estimates a tampering mask. The final output  $\hat{M}$  is a binary mask, where 0s indicate patches belonging to the pristine region and 1s indicate forged patches. If no (or just a few) forged pixels are detected, the image is considered pristine. In the following, we report a detailed explanation of each algorithmic step.

### 3.1. Feature Extraction

The first step of our algorithm consists in splitting an image into  $64 \times 64$  color patches, and extracting a feature vector containing camera model information from each one of them.

Formally, let us define with  $I(x, y)$ ,  $x \in [1, N_x]$ ,  $y \in [1, N_y]$  the pixel in position  $(x, y)$  of the image  $I$  under analysis. Similarly, let us define  $64 \times 64$  patches as  $P(i, j)$ ,  $i \in [1, N_i]$ ,  $j \in [1, N_j]$ , where  $N_i = \frac{N_x}{64}$  and  $N_j = \frac{N_y}{64}$  are the numbers of patches per column and row, respectively. In other words a patch  $P(i, j)$  corresponds to pixels  $I(x, y)$ ,  $x \in [64(i-1)+1, 64 \cdot i]$ ,  $y \in [64(j-1)+1, 64 \cdot j]$ . Each patch is fed to the pre-trained CNN presented in Section 2, which outputs a  $N_{\text{cams}}$ -dimensional feature vector  $f(i, j)$  after its Softmax layer.

Notice that features  $f(i, j)$  are vectors whose elements are positive and add to 1. Ideally, if a patch comes from a

camera model used for CNN training,  $f(i, j)$  should present a maximum close to 1 in a single position indicating the used camera model. However, in case of cameras never seen by the network, or simply due to noise,  $f(i, j)$  may present different behaviors. However, as shown in [4], this feature vector is capable of extracting camera model information that generalizes to models never used in training. Therefore, we expect that  $f(i, j)$  for patches coming from a single camera are coherent and can be clustered together in the feature space. This enables localization of pixel regions coming from different devices, even if unknown.

### 3.2. Confidence Computation

As shown in [5], the output of the used CNN is more reliable on some image patches than others. Indeed, not all patches contain enough statistical information about the used camera model. Therefore, we associate a confidence value to each patch defined as

$$Q(i, j) = \frac{1}{3} \sum_{c \in \{R, G, B\}} [\alpha \cdot \beta (\mu_c - \mu_c^2) + (1 - \alpha) (1 - e^{-\gamma \sigma_c})], \quad (1)$$

where  $\alpha$ ,  $\beta$  and  $\gamma$  are set to 0.7, 4 and  $\ln(0.01)$  in [5], whereas  $\mu_c$  and  $\sigma_c$ ,  $c \in \{R, G, B\}$  are the average and standard deviation of red, green and blue components (in range  $[0, 1]$ ) of patch  $P(i, j)$ , respectively. Notice that  $Q(i, j) \in [0, 1]$  for convenience. The lower the value, the less confident the CNN is about the patch.

### 3.3. Tampering Mask Estimation

Once we obtain confidence  $Q(i, j)$  and feature  $f(i, j)$  for each patch  $P(i, j)$ , we make use of this information to estimate a tampering mask  $\hat{M}(i, j)$ . This mask is a binary matrix, where  $\hat{M}(i, j) = 0$  indicates that  $P(i, j)$  is pristine, whereas  $\hat{M}(i, j) = 1$  indicates that  $P(i, j)$  is an alien patch.

To initialize  $\hat{M}(i, j)$ , we assume that the majority of patches come from a single camera, whereas only spliced regions come from different camera models. Therefore, the majority of vectors  $f(i, j)$  should be coherent (*i.e.* those

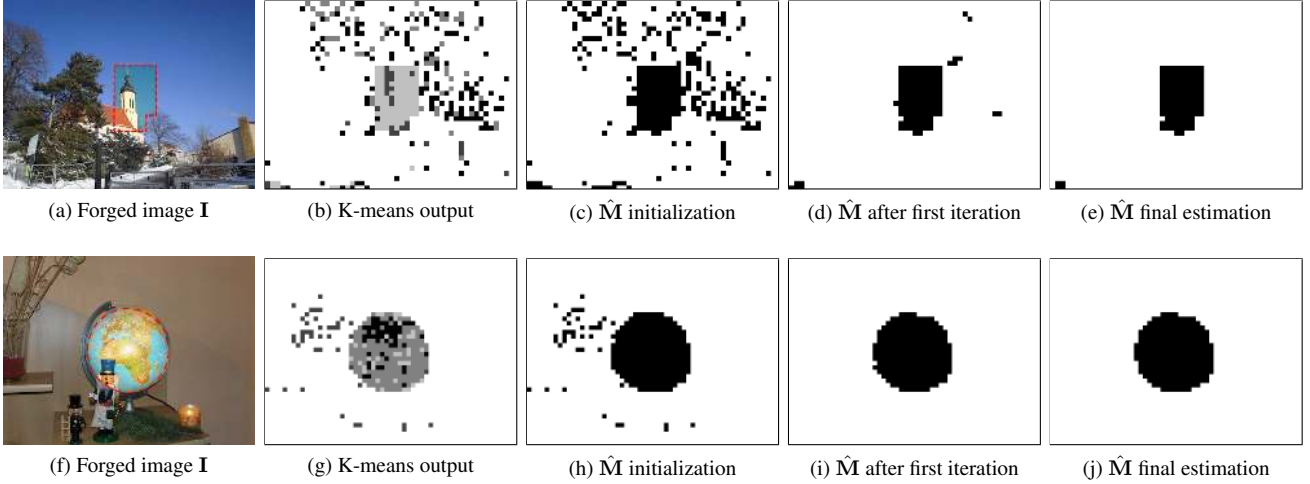


Figure 2. Example of forged images and intermediate outputs of the proposed localization algorithm. Forgeries are highlighted in red dashed lines. K-means detected clusters are mapped to different colors. White and black pixels represent 0 and 1 values of  $\hat{M}$ , respectively.

belonging to the pristine region), whereas other features should group into different clusters (*e.g.* due to noise, low confidence, or because they belong to alien regions). We therefore apply K-means clustering algorithm to features  $\mathbf{f}(i, j)$  to perform a first rough detection of which patches belong to the pristine portion of the image. In order to be robust in this initialization step, we set the initial number of clusters  $N_{\text{clusters}} = 5$  (*i.e.* greater than the expected number of cameras used for the forgery). We then set  $\hat{M}(i, j) = 0$  if  $\mathbf{f}(i, j)$  belongs to the cluster with the highest cardinality (*i.e.* pristine region). Conversely, we set  $\hat{M}(i, j) = 1$  if  $\mathbf{f}(i, j)$  belongs to any other cluster (*i.e.* possibly forged region). An example of this step output is shown for two forged images in Figure 2.

After mask initialization, we need to refine our estimate about all patches initialized as forged. To this purpose, we apply the following iterative procedure:

1. We compute the centroid  $\bar{\mathbf{f}}$  of all features  $\mathbf{f}(i, j)$  for which  $\hat{M}(i, j) = 0$  (*i.e.* pristine ones). Formally,

$$\bar{\mathbf{f}} = \text{average}(\{\mathbf{f}(i, j)\}_{(i, j) | \hat{M}(i, j)=0}), \quad (2)$$

where  $\text{average}(\cdot)$  computes the average vector in the set.

2. We compute the Bray-Curtis distance between  $\bar{\mathbf{f}}$  and each  $\mathbf{f}(i, j)$  for which  $\hat{M}(i, j) = 1$  defined as

$$\mathbf{d}(i, j) = \frac{\sum_{k=1}^{N_{\text{cams}}} |\bar{\mathbf{f}}(i, j)_k - \mathbf{f}(i, j)_k|}{\sum_{k=1}^{N_{\text{cams}}} (\bar{\mathbf{f}}(i, j)_k + \mathbf{f}(i, j)_k)}, \quad (3)$$

where  $\mathbf{f}(i, j)_k$  is the  $k$ -th element of vector  $\mathbf{f}(i, j)$ . Notice that all considered vectors add to 1, thus  $\mathbf{d}(i, j) \in [0, 1]$ .

3. We refine pristine region in the feature space by considering as pristine all patches with feature vector close to the pristine centroid  $\bar{\mathbf{f}}$ . Formally,

$$\hat{M}(i, j) = 0 \quad \text{if} \quad \mathbf{d}(i, j) < \Gamma_{\text{dist}}, \quad (4)$$

where  $\Gamma_{\text{dist}}$  is a threshold selected in range  $[0, 1]$  balancing probability of true positive and true negative detections, as shall be explained in the experimental section.

4. We finally refine pristine region estimate in the geometric space, by aggregating to pristine region spurious isolated patches considered forged. The idea is that each forgery should not be smaller than a given pixel size. Formally, we achieve this goal using opening morphological operator to  $\hat{M}$  with a  $2 \times 2$  structuring element of ones. Notice that this means we consider that the smallest possible forgery is a  $128 \times 128$  pixel region.

This procedure is iterated until convergence (*i.e.* all patches are identified as pristine, or  $\hat{M}$  estimate does not change with respect to previous step).

After last iteration, we take into account feature confidence for each patch, *i.e.*  $\mathbf{Q}(i, j)$ . Specifically, we decide to be conservative and set as pristine all patches for which we are not confident enough about their camera model estimation. Formally,

$$\hat{M}(i, j) = 0 \quad \text{if} \quad \mathbf{Q}(i, j) < \Gamma_{\text{conf}}, \quad (5)$$

where  $\Gamma_{\text{conf}}$  is a threshold selected in range  $[0, 1]$  (*i.e.* 0 means we do not take confidence into account, 1 sets all patches as pristine). For the sake of clarity, the pseudo-code is reported in Algorithm 1. Figure 2 shows an example of estimated masks for two forged images.

### 3.4. Tampering Detection

Once mask  $\hat{\mathbf{M}}$  has been estimated, we decide whether image  $\mathbf{I}$  is pristine or not based on the amount of estimated forged pixels. Formally,

$$\begin{cases} \mathbf{I} \text{ is pristine} & \text{if } \mu_{\hat{\mathbf{M}}} \leq \Gamma_{\text{det}}, \\ \mathbf{I} \text{ is forged} & \text{if } \mu_{\hat{\mathbf{M}}} > \Gamma_{\text{det}}, \end{cases} \quad (6)$$

where  $\mu_{\hat{\mathbf{M}}}$  is the average value of  $\hat{\mathbf{M}}$  which spans the range  $[0, 1]$ , and  $\Gamma_{\text{det}}$  is a threshold indicating how many pixels we need to identify as forged to estimate that the image is actually forged (*i.e.* 0 means that images are considered pristine only if all patches are detected as pristine, 1 means that images are always considered pristine).

## 4. Experimental Results

In this section we present all achieved experimental results. To this purpose, we first present the used dataset. Then, we provide implementation details about CNN training procedure. Finally, we report numeric results on tampering detection and tampering localization, also comparing against different state-of-the-art methods [43].

### 4.1. Dataset

The reference dataset used to validate the proposed method is the Dresden Image Database [16]. The dataset consist of more than 16k images from 26 different camera models depicting a total of 83 scenes. As suggested in [21] *Nikon D70* and *Nikon D70s* are considered as the same camera model. In a first phase aimed at training the CNN, the 18 camera models with more than one device per model are taken into account and split into a training  $\mathcal{D}_T$ , validation  $\mathcal{D}_V$ , and evaluation  $\mathcal{D}_E$  sets. One camera instance per model is selected for  $\mathcal{D}_E$ , whereas all other camera instances are in  $\mathcal{D}_T$  and  $\mathcal{D}_V$ . Shots from same scene (*e.g.* outdoor, indoor, etc.) are only in one of the three sets. This replicates the splitting strategy adopted in [4], aimed at avoiding that the CNN trained on  $\mathcal{D}_T$  and  $\mathcal{D}_V$  over-fits on image content rather than learning camera specific features.

In a second phase two distinct tampered datasets are generated: i) the *known* dataset made from images in  $\mathcal{D}_E$ , and; ii) the *unknown* dataset containing images from the 8 single instance camera models never seen by the CNN. It is important in our opinion to evaluate our algorithm on both datasets to study performance differences in case known or unknown cameras are used. Indeed, working with camera models known by the CNN should be a more favorable working condition. However, it is important that the algorithm shows robust also to unknown cameras.

Both *known* and *unknown* datasets contain 500 pristine images and 500 tampered images generated according to the following procedure:

#### Algorithm 1: Tampering mask estimation

```

Data: Feature vectors  $\mathbf{f}(i, j)$ ,  $i \in [1, N_i]$ ,  $j \in [1, N_j]$ 
Confidence  $\mathbf{Q}(i, j)$ ,  $i \in [1, N_i]$ ,  $j \in [1, N_j]$ 

Input: Thresholds  $\Gamma_{\text{dist}}$  and  $\Gamma_{\text{conf}}$ 
Kmeans number of clusters  $N_{\text{clusters}}$ 

Output: Tampering mask  $\hat{\mathbf{M}}$ 

begin
// Mask initialization
cluster( $i, j$ ) = Kmeans( $\{\mathbf{f}(i, j)\}_{\forall(i, j)}$ ,  $N_{\text{clusters}}$ )
foreach ( $i, j$ ) do
| if cluster( $i, j$ ) is the largest one then
| |  $\hat{\mathbf{M}}(i, j) = 0$ 
| else
| |  $\hat{\mathbf{M}}(i, j) = 1$ 
| end
end

// Refinement procedure
do
| // Centroid estimation
|  $\bar{\mathbf{f}} = \text{average}(\{\mathbf{f}(i, j)\}_{(i, j) | \hat{\mathbf{M}}(i, j)=0})$ 
| // Feature space refinement
| foreach ( $i, j$ ) |  $\hat{\mathbf{M}}(i, j) = 1$  do
| |  $\mathbf{d}(i, j) = \frac{\sum_{k=1}^{N_{\text{cams}}} |\bar{\mathbf{f}}(i, j)_k - \mathbf{f}(i, j)_k|}{\sum_{k=1}^{N_{\text{cams}}} (\bar{\mathbf{f}}(i, j)_k + \mathbf{f}(i, j)_k)}$ 
| | if  $\mathbf{d}(i, j) < \Gamma_{\text{dist}}$  then
| | |  $\hat{\mathbf{M}}(i, j) = 0$ 
| | end
| end

| // Geometric space refinement
|  $\hat{\mathbf{M}} = \text{opening}(\hat{\mathbf{M}})$ 

while  $\hat{\mathbf{M}}$  changes from previous iteration

// Confidence thresholding
foreach ( $i, j$ ) do
| if  $\mathbf{Q}(i, j) < \Gamma_{\text{conf}}$  then
| |  $\hat{\mathbf{M}}(i, j) = 0$ 
| end
end
end

```

1. Select a random receiver image  $\mathbf{I}_{\text{rcv}}$  from the dataset.
2. Generate an empty mask  $\mathbf{M}$  with the same size of  $\mathbf{I}_{\text{rcv}}$ .
3. Randomly chose the number of donor alien images  $N_d$  in  $[1, 2]$ .
4. For each donor  $d \in [1, N_d]$ :
  - Select a random donor image  $\mathbf{I}_{\text{dnr}}^d$  from the dataset, taking care it comes from a different camera model than  $\mathbf{I}_{\text{rcv}}$ .
  - Copy a rectangular random region with width and

height in  $[128, 1024]$  from  $\mathbf{I}_{\text{dnr}}^d$  and paste it in a random location of  $\mathbf{I}_{\text{rcv}}$  (not paying attention to any grid alignment).

- Update  $\mathbf{M}$  accordingly.

5. Store  $\mathbf{I}_{\text{rcv}}$  and  $\mathbf{M}$  as forged image and ground-truth mask.

## 4.2. CNN training and feature extraction

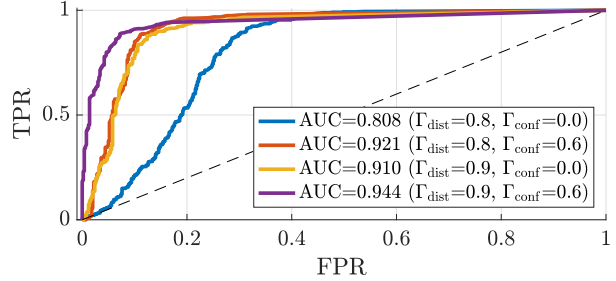
The first step toward feature extraction is training the CNN architecture described in Section 2. From each image in  $\mathcal{D}_T$  and  $\mathcal{D}_V$  we extracted the 32 highest scoring  $64 \times 64$  patches according to the confidence function (1). Patches from  $\mathcal{D}_T$  are fed to the CNN in batch of 128, training the network with back-propagation based on Stochastic Gradient Descent with momentum 0.9, weights decay set to  $7.5 \cdot 10^{-3}$  and exponentially decreasing learning rate starting from 0.01. After every training epoch we compute the average loss on validation patches extracted from  $\mathcal{D}_V$  and we stop the training process as validation loss converges to its minimum value. Notice that the CNN is only trained on pristine images.

Once the CNN is trained, each image  $\mathbf{I}$  from the *known* and the *unknown* dataset is split into non overlapping  $64 \times 64$  patches. Each patch  $\mathbf{P}(i, j)$  is fed to the CNN and the Softmax layer output is used as a feature vector  $\mathbf{f}(i, j)$  relative to  $\mathbf{P}(i, j)$ .

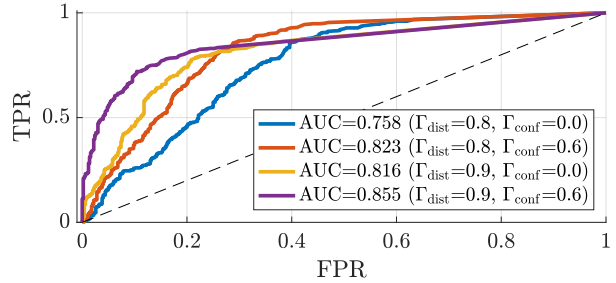
## 4.3. Tampering Detection

The proposed algorithm for tampering detection depends on three thresholds (*i.e.*  $\Gamma_{\text{dist}}$ ,  $\Gamma_{\text{conf}}$  and  $\Gamma_{\text{det}}$ ), all taking values in range  $[0, 1]$ . Figure 3 shows detection performance on both *known* and *unknown* datasets in terms of receiver operating characteristic (ROC) curves moving detection threshold  $\Gamma_{\text{det}}$  and fixing  $\Gamma_{\text{dist}}$  and  $\Gamma_{\text{conf}}$ . Results in terms of area under the curve (AUC) show that, on both datasets, the best detection performance are obtained for  $\Gamma_{\text{dist}} = 0.9$  and  $\Gamma_{\text{conf}} = 0.6$ . Using  $\Gamma_{\text{dist}}$  close to 1 means that we only consider as forged, patches whose feature vector is pretty far from the estimated pristine centroid. Using  $\Gamma_{\text{conf}} \neq 0$  means that taking into account confidence score  $\mathbf{Q}(i, j)$  actually helps refining detection results.

However, as the role of  $\Gamma_{\text{det}}$  is to decide how many forged blocks should be detected in an image in order to decide that the picture is forged, we also computed some additional results by setting  $\Gamma_{\text{det}} = 0$ . This case means we only detect as pristine, images for which  $\hat{\mathbf{M}}(i, j) = 0$  for all  $(i, j)$ . Table 1 shows results in terms of: i) true positive rate (TPR), *i.e.* the percentage of forged images correctly detected as such; ii) true negative rate (TNR), *i.e.* the percentage of pristine images correctly detected as such; iii) accuracy (ACC), *i.e.* the average between TPR and TNR. threshold  $\Gamma_{\text{det}} = \text{best}$ , means we selected  $\Gamma_{\text{det}}$  values maximizing accuracy according to ROC results. Notice that, setting  $\Gamma_{\text{det}} = 0$  always



(a) *known* dataset



(b) *unknown* dataset

Figure 3. ROC curves of tampering detection algorithm tested on *known* (a) and *unknown* (b) datasets using different thresholds  $\Gamma_{\text{dist}}$  and  $\Gamma_{\text{conf}}$  values.

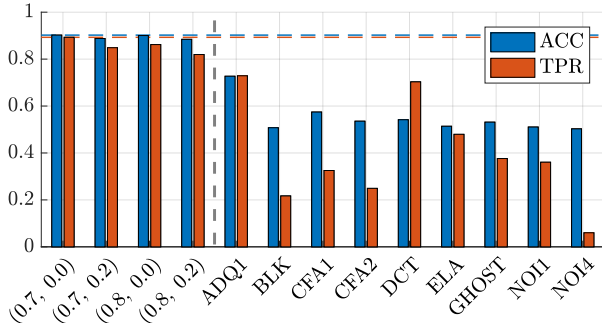
Table 1. Tampering detection results.  $\Gamma_{\text{det}} = \text{best}$  is the threshold maximizing accuracy.

Dataset	$\Gamma_{\text{dist}}$	$\Gamma_{\text{conf}}$	$\Gamma_{\text{det}}$	ACC	TPR	TNR
<i>known</i>	0.8	0.0	0	0.720	<b>0.994</b>	0.446
			best	<b>0.800</b>	0.914	<b>0.686</b>
	0.8	0.6	0	0.832	<b>0.980</b>	0.684
			best	<b>0.888</b>	0.916	<b>0.860</b>
0.9	0.0	0	0.823	<b>0.966</b>	0.680	
		best	<b>0.877</b>	0.878	<b>0.876</b>	
0.9	0.6	0	0.890	<b>0.942</b>	0.838	
		best	<b>0.908</b>	0.888	<b>0.928</b>	
<i>unknown</i>	0.8	0.0	0	0.668	<b>0.968</b>	0.368
			best	<b>0.731</b>	0.860	<b>0.602</b>
	0.8	0.6	0	0.742	<b>0.954</b>	0.530
			best	<b>0.784</b>	0.856	<b>0.712</b>
0.9	0.0	0	0.741	<b>0.864</b>	0.618	
		best	<b>0.785</b>	0.786	<b>0.784</b>	
0.9	0.6	0	0.788	<b>0.834</b>	0.742	
		best	<b>0.810</b>	0.772	<b>0.848</b>	

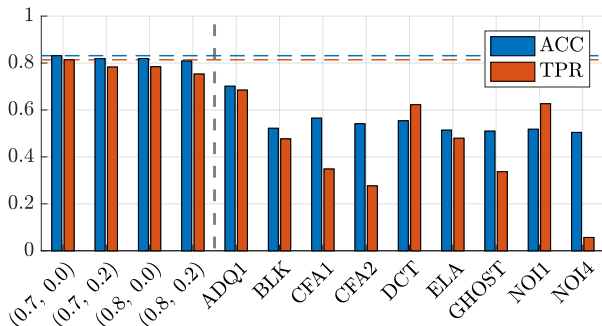
provide better TPR results, albeit a different threshold (*i.e.* the one maximizing accuracy) is more suitable to balance TPR and TNR.

## 4.4. Tampering Localization

As far as tampering localization is concerned, we compared the proposed algorithm on forged images against nine methods reviewed in [43], whose implementation were



(a) known dataset



(b) unknown dataset

Figure 4. Accuracy and TPR on *known* (a) and *unknown* (b) datasets using our algorithm (left hand side of dashed line) with different thresholds ( $\Gamma_{\text{dist}}$ ,  $\Gamma_{\text{conf}}$ ) and state-of-the-art algorithms (right hand side of dashed gray line). Our best accuracy and TPR results are reported with dashed blue and orange lines.

made available in the toolbox presented in the same paper. More specifically, we took into account all algorithms presented in Section 2, as they do not need any additional prior information on images under analysis (*e.g.* PRNUs, JPEG quantization matrix, etc.).

As evaluation metrics, we decided to rely on: i) true positive rate (TPR), *i.e.* the percentage of forged pixels correctly detected as such; ii) balanced accuracy (ACC), *i.e.* the average between TPR and the percentage of correctly detected pristine pixels. However, differently from our method, state-of-the-art considered ones output a float tampering mask. In order to enable a fair comparison, we binarized float masks using the threshold that maximizes each state-of-the-art algorithm accuracy.

Figure 4 shows results obtained with our method for different values of thresholds  $\Gamma_{\text{dist}}$  and  $\Gamma_{\text{conf}}$ , together with state-of-the-art methods. Notice that, our method achieves best results when  $\Gamma_{\text{conf}} = 0$ . This means that for localization purpose, it is better to discard confidence  $Q(i, j)$  information, which instead turned to be paramount for detection purpose. Regarding comparison against state-of-the-art, it is possible to notice that our algorithm outperforms all considered baseline solutions. This is due to the fact that con-

sidered baselines are tailored to different kinds of tampering operations. Even more interesting, the proposed method achieves promising results even on the *unknown* dataset. This means that we are able to cope with composition forgeries even when used cameras do not belong to the CNN training set. Moreover, it is possible to notice that even by slightly varying thresholds  $\Gamma_{\text{dist}}$  and  $\Gamma_{\text{conf}}$ , our results do not drop under baselines performance, showing a good degree of robustness also to the choice of sub-optimal parameters.

## 5. Conclusions

In this paper we presented an algorithm for tampering detection and localization to expose splicing forgeries operated using images from different camera models. The proposed method exploits a CNN to extract features capturing camera model traces from image patches. Features are clustered into two groups (*i.e.* pristine or forged) using an iterative algorithm, and information about patches locations is further used to refine forgery localization estimation.

Evaluation carried out on a dataset of 2 000 images obtained from 26 camera models shows that the proposed algorithm is able to detect forged images with accuracy of 0.91 if camera models involved in forgeries have been used during CNN training. If camera models involved in forgeries have never been used for training, detection accuracy still remains as high as 0.81. Results on tampering localization shows that it is possible to detect forged regions with accuracy about 0.90 and 0.82 depending on the knowledge (or not) of the used camera models at training stage. This makes the proposed method more accurate than alternative baseline solutions selected from [43].

Future work will follow two parallel research lines. On one hand, we will explore the possibility of specializing the used CNN to learn characteristics of additional processing steps in addition to traces of camera models (*e.g.* resizing, rotations, blurring, etc.). On the other hand, we will study how to use CNN capabilities directly for localization purpose by training also on forged images.

## Acknowledgment

This material is based on research sponsored by DARPA and Air Force Research Laboratory (AFRL) under agreement number FA8750-16-2-0173. The U.S. Government is authorized to reproduce and distribute reprints for Governmental purposes notwithstanding any copyright notation thereon. The views and conclusions contained herein are those of the authors and should not be interpreted as necessarily representing the official policies or endorsements, either expressed or implied, of DARPA and Air Force Research Laboratory (AFRL) or the U.S. Government.



## References

- [1] E. Ardizzone, A. Bruno, and G. Mazzola. Copy Move Forgery Detection by Matching Triangles of Keypoints. *IEEE Transactions on Information Forensics and Security (TIFS)*, 10:2084–2094, 2015.
- [2] B. Bayar and M. C. Stamm. A Deep Learning Approach To Universal Image Manipulation Detection Using A New Convolutional Layer. In *Information Hiding and Multimedia Security*, 2016.
- [3] T. Bianchi and A. Piva. Detection of nonaligned double JPEG compression based on integer periodicity maps. *IEEE Transactions on Information Forensics and Security (TIFS)*, 7:842–848, 2012.
- [4] L. Bondi, L. Baroffio, D. Güera, P. Bestagini, E. J. Delp, and S. Tubaro. First Steps Toward Camera Model Identification With Convolutional Neural Networks. *IEEE Signal Processing Letters (SPL)*, 24:259–263, 2017.
- [5] L. Bondi, D. Güera, L. Baroffio, P. Bestagini, E. J. Delp, and S. Tubaro. A preliminary study on convolutional neural networks for camera model identification. In *IS&T Electronic Imaging (EI)*, 2017.
- [6] G. Cao, Y. Zhao, R. Ni, L. Yu, and H. Tian. Forensic detection of median filtering in digital images. In *IEEE International Conference on Multimedia and Expo (ICME)*, 2010.
- [7] J. Chen, X. Kang, Y. Liu, and Z. J. Wang. Median Filtering Forensics Based on Convolutional Neural Networks. *IEEE Signal Processing Letters (SPL)*, 22:1849–1853, 2015.
- [8] V. Conotter, P. Comesana, and F. Perez-Gonzalez. Forensic analysis of full-frame linearly filtered JPEG images. In *IEEE International Conference on Image Processing (ICIP)*, 2013.
- [9] D. Cozzolino and G. Poggi. Autoencoder with recurrent neural networks for video forgery detection Autoencoder with recurrent neural networks for video forgery detection. In *IS&T Electronic Imaging (EI)*, 2017.
- [10] D. Cozzolino and L. Verdoliva. Single-image splicing localization through autoencoder-based anomaly detection. In *IEEE International Workshop on Information Forensics and Security (WIFS)*, 2016.
- [11] A. E. Dirik and N. Memon. Image tamper detection based on demosaicing artifacts. In *IEEE International Conference on Image Processing (ICIP)*, 2009.
- [12] H. Farid. Exposing Digital Forgeries From JPEG Ghosts. *IEEE Transactions on Information Forensics and Security (TIFS)*, 4:154–160, 2009.
- [13] P. Ferrara, T. Bianchi, A. De Rosa, and A. Piva. Image forgery localization via fine-grained analysis of CFA artifacts. *IEEE Transactions on Information Forensics and Security (TIFS)*, 7:1566–1577, 2012.
- [14] M. Fontani, S. Member, T. Bianchi, and A. D. Rosa. A Framework for Decision Fusion in Image Forensics Based on Dempster Shafer Theory of Evidence. *IEEE Transactions on Information Forensics and Security (TIFS)*, 8:593–607, 2013.
- [15] L. Gaborini, P. Bestagini, S. Milani, M. Tagliasacchi, and S. Tubaro. Multi-clue image tampering localization. In *IEEE International Workshop on Information Forensics and Security (WIFS)*, 2015.
- [16] T. Gloe and R. Böhme. The Dresden Image Database for Benchmarking Digital Image Forensics. *Journal of Digital Forensic Practice*, 3:150–159, 2010.
- [17] M. Goljan and J. Fridrich. Camera identification from cropped and scaled images. In *SPIE Electronic Imaging (EI)*, 2008.
- [18] J. Hosang, M. Omran, R. Benenson, and B. Schiele. Taking a deeper look at pedestrians. In *IEEE Conference on Computer Vision and Pattern Recognition (CVPR)*, 2015.
- [19] M. Kirchner. Fast and reliable resampling detection by spectral analysis of fixed linear predictor residue. In *ACM workshop on Multimedia and Security (MM&Sec)*, 2008.
- [20] M. Kirchner and J. Fridrich. On detection of median filtering in digital images. In *SPIE Media Forensics and Security*, 2010.
- [21] M. Kirchner and T. Gloe. Forensic Camera Model Identification. In *Handbook of Digital Forensics of Multimedia Data and Devices*. John Wiley & Sons, Ltd, 2015.
- [22] N. Krawetz. A Picture’s Worth... *Hacker Factor Solutions*, pages 1–31, 2007.
- [23] A. Krizhevsky, I. Sutskever, and G. E. Hinton. ImageNet Classification with Deep Convolutional Neural Networks. *Advances in Neural Information and Processing Systems (NIPS)*, pages 1–9, 2012.
- [24] Y. LeCun, L. Bottou, Y. Bengio, and P. Haffner. Gradient-based learning applied to document recognition. *Proceedings of the IEEE*, 86:2278–2323, 1998.
- [25] W. Li, Y. Yuan, and N. Yu. Passive detection of doctored JPEG image via block artifact grid extraction. *Signal Processing*, 89:1821–1829, 2009.
- [26] M. Lin, Q. Chen, and S. Yan. Network In Network. *arXiv preprint*, page 10, 2013.
- [27] Z. Lin, J. He, X. Tang, and C. K. Tang. Fast, automatic and fine-grained tampered JPEG image detection via DCT coefficient analysis. *Pattern Recognition*, 42:2492–2501, 2009.
- [28] J. Lukas, J. Fridrich, and M. Goljan. Determining digital image origin using sensor imperfections. In *Proceedings of the SPIE*, 2005.
- [29] J. Lukas, J. Fridrich, and M. Goljan. Digital Camera Identification From Sensor Pattern Noise. *IEEE Transactions on Information Forensics and Security (TIFS)*, 1:205–214, 2006.
- [30] B. Mahdian and S. Saic. Using noise inconsistencies for blind image forensics. *Image and Vision Computing*, 27:1497–1503, 2009.
- [31] A. Piva. An overview on image forensics. *ISRN Signal Processing*, 2013:22, 2013.
- [32] A. Popescu and H. Farid. Exposing digital forgeries by detecting traces of resampling. *IEEE Transactions on Signal Processing (TSP)*, 53:758–767, 2005.
- [33] Y. Qian, J. Dong, W. Wang, and T. Tan. Deep learning for steganalysis via convolutional neural networks. In *SPIE Media Watermarking, Security, and Forensics*, 2015.
- [34] A. Rocha, W. Scheirer, T. Boulton, and S. Goldenstein. Vision of the unseen: Current trends and challenges in digital image and video forensics. *ACM Computing Surveys*, 43:1–42, 2011.

- [35] M. C. Stamm, Min Wu, and K. J. R. Liu. Information Forensics: An Overview of the First Decade. *IEEE Access*, 1:167–200, 2013.
- [36] C. Szegedy, W. Liu, Y. Jia, and P. Sermanet. Going deeper with convolutions. In *IEEE Conference on Computer Vision and Pattern Recognition (CVPR)*, 2015.
- [37] Y. Taigman, M. Yang, M. Ranzato, and L. Wolf. DeepFace: Closing the Gap to Human-Level Performance in Face Verification. In *IEEE Conference on Computer Vision and Pattern Recognition (CVPR)*, 2014.
- [38] T. H. Thai, R. Cogranne, F. Reiraint, and T.-N.-C. Doan. JPEG Quantization Step Estimation and Its Applications to Digital Image Forensics. *IEEE Transactions on Information Forensics and Security (TIFS)*, 12:123–133, 2017.
- [39] D. Tomè, F. Monti, L. Baroffio, L. Bondi, M. Tagliasacchi, and S. Tubaro. Deep Convolutional Neural Networks for pedestrian detection. *Signal Processing: Image Communication*, 47:482–489, 2016.
- [40] A. Tuama, F. Comby, and M. Chaumont. Camera model identification with the use of deep convolutional neural networks. In *IEEE International Workshop on Information Forensics and Security (WIFS)*, 2016.
- [41] L. Verdoliva, D. Cozzolino, and G. Poggi. A feature-based approach for image tampering detection and localization. In *IEEE International Workshop on Information Forensics and Security (WIFS)*, 2014.
- [42] S. Ye, Q. Sun, and E.-C. Chang. Detecting Digital Image Forgeries by Measuring Inconsistencies of Blocking Artifact. In *IEEE International Conference on Multimedia and Expo (ICME)*, volume 117543, 2007.
- [43] M. Zampoglou, S. Papadopoulos, and Y. Kompatsiaris. Large-scale evaluation of splicing localization algorithms for web images. *Multimedia Tools and Applications*, 76(4):4801–4834, feb 2017.